arXiv:2511.16567v3 [cs.CV] 6 May 2026

POMA-3D: The Point Map Way to 3D Scene Understanding

Ye Mao Weixun Luo Ranran Huang Junpeng Jing[†] Krystian Mikolajczyk

Imperial College London

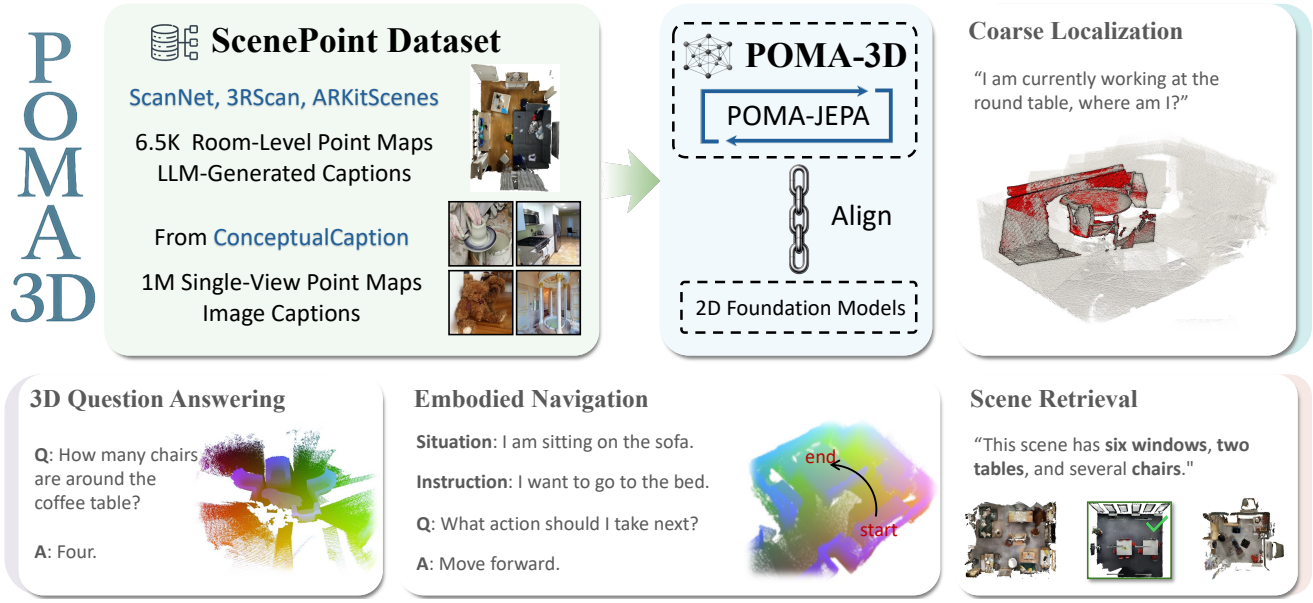

Figure 1. **Overview of POMA-3D.** POMA-3D is a self-supervised 3D model pretrained on the large-scale point map dataset ScenePoint via alignment with 2D foundation models and the POMA-JEPA objective. The 3D features from pretrained POMA-3D generalize to diverse 3D scene understanding tasks, including 3D question answering, embodied navigation, scene retrieval, and coarse localization.

Abstract

In this paper, we introduce POMA-3D, the first self-supervised 3D representation model learned from point maps. Point maps encode explicit 3D coordinates on a structured 2D grid, preserving global 3D geometry while remaining compatible with the input format of 2D foundation models. To transfer rich 2D priors into POMA-3D, a view-to-scene alignment strategy is designed. Moreover, as point maps are view-dependent with respect to a canonical space, we introduce POMA-JEPA, a joint embedding-predictive architecture that enforces geometrically consistent point map features across multiple views. Additionally, we introduce ScenePoint, a point map dataset constructed from 6.5K room-level RGB-D scenes and 1M 2D image scenes to facilitate large-scale POMA-3D pretraining. Experiments show that POMA-3D serves as a strong backbone for both specialist and generalist 3D understanding. It benefits diverse tasks, including 3D question answering, embodied navigation, scene retrieval, and coarse localization, all achieved using only geometric inputs (i.e., 3D coordinates). Overall, our POMA-3D explores a ***point map way to 3D scene understanding****, addressing the scarcity of pretrained priors and limited data in 3D representation learning. Code and dataset are publicly available at https://matchlab-imperial.github.io/poma3d/.*

[†]Corresponding author: j.jing23@imperial.ac.uk

1. Introduction

Understanding 3D scenes is fundamental for perceiving and interacting with the physical world, forming the basis of contextual intelligence in AR systems and embodied agents [13, 29]. Early 3D understanding models were specialist, targeting specific 3D tasks such as instance segmentation [19, 25], visual grounding [1, 8], or visual question answering (QA) [4, 33]. Recently, generalist 3D models [9, 15, 16, 46, 54, 57] have emerged, leveraging large

language models (LLMs) to achieve holistic 3D understanding across diverse tasks within a unified framework.

Both specialist and generalist models hinge on robust spatial representations. 3D vision-language learning (VLL) provide them through contrastive objectives without relying on downstream annotations. Early 3D VLL methods align trainable 3D encoders with frozen 2D vision-language models (e.g., CLIP [40]). This cross-modal alignment enables 3D encoders to inherit rich knowledge from 2D counterparts, enabling zero-shot tasks such as object classification, retrieval, and detection [31, 35, 39, 51, 52, 56]. Subsequent methods [24, 59] extend this paradigm from object to scene-level representation learning. However, existing 3D VLL methods have yet to achieve a breakthrough comparable to the CLIP moment in 2D understanding.

The key reason is that these methods primarily utilize point clouds [24, 59], depth maps [23, 35], or 3D Gaussian splatting [28, 44] for alignment, all of which differ substantially from pretrained 2D representations. *In this paper, we argue that point maps can provide a superior intermediate 2D–3D modality for better alignment.* This is enabled by recent advances in feed-forward 3D reconstruction models [21, 26, 47, 48]. Unlike other 3D inputs, point maps encodes pixel-to-3D correspondences in a 2D grid, naturally naturally matching the data format of 2D foundational models. Moreover, multi-view point maps are defined in canonical world coordinates, preserving the same global geometry as point clouds. These properties collectively make point maps a promising modality that retains rich 3D information while aligning closer with 2D knowledge.

Motivated by these properties, we introduce POMA-3D, the first self-supervised 3D learning framework built upon point maps, as illustrated in Fig. 1. To enable large-scale pretraining, we construct ScenePoint, a point map dataset comprising over 6.5K room-level indoor scenes paired with LLM-generated descriptions. In addition, we convert 1M images from image-caption datasets into single-view point maps using the VGGT model [47] for 3D learning. Building on ScenePoint, POMA-3D is pretrained with a view-to-scene vision–language alignment objective, encouraging the model to learn CLIP-aligned point map embeddings. To ensure feature consistency across viewpoints, we further design the Point Map Joint Embedding-Predictive Architecture (POMA-JEPA) as an additional training objective. Unlike traditional JEPAs [2, 3, 6], POMA-JEPA explicitly handles the order-agnostic nature of point maps in the world coordinate frame by enforcing permutation-invariant embedding prediction. The overall training follows a two-stage paradigm: a warm-up stage using 2D image scenes, followed by a main stage using indoor room scenes.

We evaluate the generalizability of POMA-3D across diverse 3D scene understanding tasks, including 3D question answering, embodied navigation, and scene retrieval. After pretraining, POMA-3D gains the ability to accurately locate the agent's active region from textual queries in a zero-shot setting, a task we term coarse localization (see Fig. 1). When used as a backbone for both specialist and generalist 3D models, POMA-3D consistently outperforms existing state-of-the-art 3D VLL methods, even without color information—using only pure 3D coordinates. Notably, our results demonstrate that leveraging 2D vision–language data significantly benefits POMA-3D pretraining, highlighting a promising direction toward addressing the long-standing data scarcity challenge in building foundation models for 3D understanding.

Our contributions can be summarized as follows:

- We propose POMA-3D, the first self-supervised model that learns 3D scene representations from point maps.
- We present ScenePoint, a large-scale point map dataset comprising 6.5K room-level and 1M image scenes for POMA-3D two-stage pretraining.
- We design a view-to-scene vision–language alignment and POMA-JEPA as training objectives to learn CLIP-aligned and multi-view consistent point map features.

2. Related Work

From Specialist to Generalist 3D Models. Existing 3D scene understanding methods fall into specialist and generalist paradigms. Specialist models [8, 17, 19, 22, 25, 38, 53] are tailored for individual tasks such as segmentation or grounding, achieving strong performance but limited cross-task generalization. Building on advances in large language models (LLMs), recent 3D generalist models aim to unify perception and reasoning across modalities. Early efforts such as 3D-LLM [18] adapt LLMs to process 3D features from rendered images, while Chat3D [49] and LEO [20] enhance 3D reasoning by integrating object-centric representations from off-the-shelf 3D detectors. LLaVA-3D [57] extends 2D visual instruction tuning to 3D via voxelized patch aggregation, and Video-3D LLM [54] incorporates 3D cues into video-based representations. SR-3D [10] is the most related work to ours, using point maps to build a generalist 3D model. However, it uses point maps only as a source of 3D positional encoding rather than pretraining a dedicated encoder to learn point map representations. In this work, we propose POMA-3D, which learns generalizable point map features that effectively benefit both specialist and generalist models across diverse 3D understanding tasks.

3D Vision-Language Learning. Existing 3D vision-language learning (VLL) methods align 3D data (e.g., point clouds, depth maps, voxel grids), multi-view images, and text through contrastive objectives, transferring rich semantic priors from CLIP into 3D domains. Early works such as ULIP [51], OpenShape [31], OpenDlign [35], and Uni3D [56] demonstrate that CLIP-based supervision produces strong 3D object representations for open-world

Table 1. Comparison of ScenePoint with existing indoor 3D vision-language datasets. "CC" for ConceptualCaptions [43].

Dataset/Attribute	SceneScribe [59]	SceneVerse [24]	ScenePoint
ScanNet [11]	✓	✓	✓
ARKitScenes [7]	✗	✓	✓
HM3D [41]	✗	✓	✗
3RScan [45]	✓	✓	✓
MultiScan [34]	✗	✓	✗
Structured3D [55]	✗	✓	✗
ProcTHOR [12]	✗	✓	✗
CC [43]	✗	✗	✓
Caption Detail	Object, Scene	Object, Scene	**View, Scene**
Room-level Scene	3.0K	68K	**6.5K**
Single-view Scene	–	–	**1M**

recognition and retrieval. However, these approaches remain object-centric, limiting their ability to capture holistic scene semantics. To address this limitation, 3D-VisTA [59] extends VLL to 3D scenes by aligning scene-level point cloud features with scene captions, while SceneVerse [24] scales this approach to a large corpus of 3D scenes, yielding promising results in 3D visual grounding. More recently, SceneSplat [28] explores VLL on 3D Gaussian splats, producing continuous 3D features that enhance scene segmentation. Building on this line of research, POMA-3D also adopts vision-language alignment as a key training objective. Unlike prior scene-based methods that focus on object- or scene-level alignment, POMA-3D aligns point map view and scene representations, as summarized in Tab. 1.

3D Scene Pretraining Datasets. Collecting large-scale 3D scene data for 3D vision-language learning remains a major challenge due to the high cost and prolonged scanning time required by 3D sensing devices. Widely used datasets such as ScanNet [11], 3RScan [45], ARKitScenes [7], HM3D [41], and MultiScan [34] contain only thousands of scenes, which is much smaller than the billion-scale image text corpora used for 2D pretraining. To mitigate this limitation, several works [24] have leveraged synthetic 3D scene datasets such as Structured3D [55] and ProcTHOR [12]. However, the limited realism of synthetic scenes restricts their effectiveness in learning generalizable real-world representations. In this work, we leverage 2D vision–language datasets for 3D learning by using a feed-forward 3D model to convert images into pseudo point maps, enabling scalable 3D vision-language learning.

3. ScenePoint Dataset

We introduce ScenePoint, a dataset of aligned triplets consisting of point maps, images, and captions of 3D indoor scenes for vision-language point map pretraining. As summarized in Tab. 1, ScenePoint integrates diverse RGB-D scene datasets, each annotated with both LLM-generated view-level and scene-level captions. In addition, it includes single-view scenes generated from image caption datasets.

3.1. Point Map Curation

Multi-view point maps are constructed from RGB-D room videos by sampling 32 frames per video. Following the maximum sampling coverage strategy of Video-3D-LLM [54], the selected frames capture the maximum spatial extent of each scene. Each point map view P_i is generated from its corresponding depth map $D_i \in \mathbb{R}^{H\times W}$ using the intrinsic matrix K and the extrinsic parameters $E_i = [R_i \,|\, t_i]$, where R_i and t_i represent rotation and translation, respectively. The resulting point map $P_i \in \mathbb{R}^{H\times W\times 3}$ preserves the spatial resolution of D_i, where each pixel in (u, v) stores its 3D coordinate (x, y, z) as:

$$\begin{bmatrix} x \\ y \\ z \end{bmatrix} = R_i \left(D_i(u,v) K^{-1} \begin{bmatrix} u \\ v \\ 1 \end{bmatrix} \right) + t_i. \tag{1}$$

Single-view point maps are generated from images in the ConceptualCaptions dataset [43] using Eq. 1, where depth maps and camera parameters are predicted by the depth and pose heads of the VGGT model [47].

3.2. Language Generation

Language annotations are provided at both the view and scene levels of the point maps. For room-level point maps, each view is paired with captions generated by InternVL3-14B [58], using the corresponding RGB image as input. Specifically, 15 candidate captions $\{c_j\}_{j=1}^{15}$ are first produced, and their cosine similarities with the corresponding FG-CLIP [50] image embedding f^{img} are computed as $s_j = \cos(f^{\text{img}}, f^{\text{text}}_{c_j})$. The top-5 captions with the highest s_j are retained as the final view-level annotations. Scene-level captions for room-level point maps are adopted from SceneVerse [24]. For single-view point maps, the original image captions are directly used as their view-level annotations.

3.3. Dataset Statistics

Tab. 1 shows that ScenePoint comprises 6,562 indoor scenes collected from three RGB-D datasets, including 1,499 from ScanNet [11], 1,204 from 3RScan [45], and 3,850 from ARKitScenes [7]. Unlike previous datasets, ScenePoint does not include any synthetic 3D scenes. Instead, it incorporates 1M image scenes sampled from the ConceptualCaptions [43] dataset.

4. POMA-3D

The overall pretraining framework of POMA-3D is illustrated in Fig. 2. Built upon the ScenePoint dataset, POMA-3D is trained with two objectives: (1) *view-to-scene vision–language alignment* (Sec. 4.1) to align point map, image, and text embeddings, and (2) *POMA-JEPA* (Sec. 4.2)

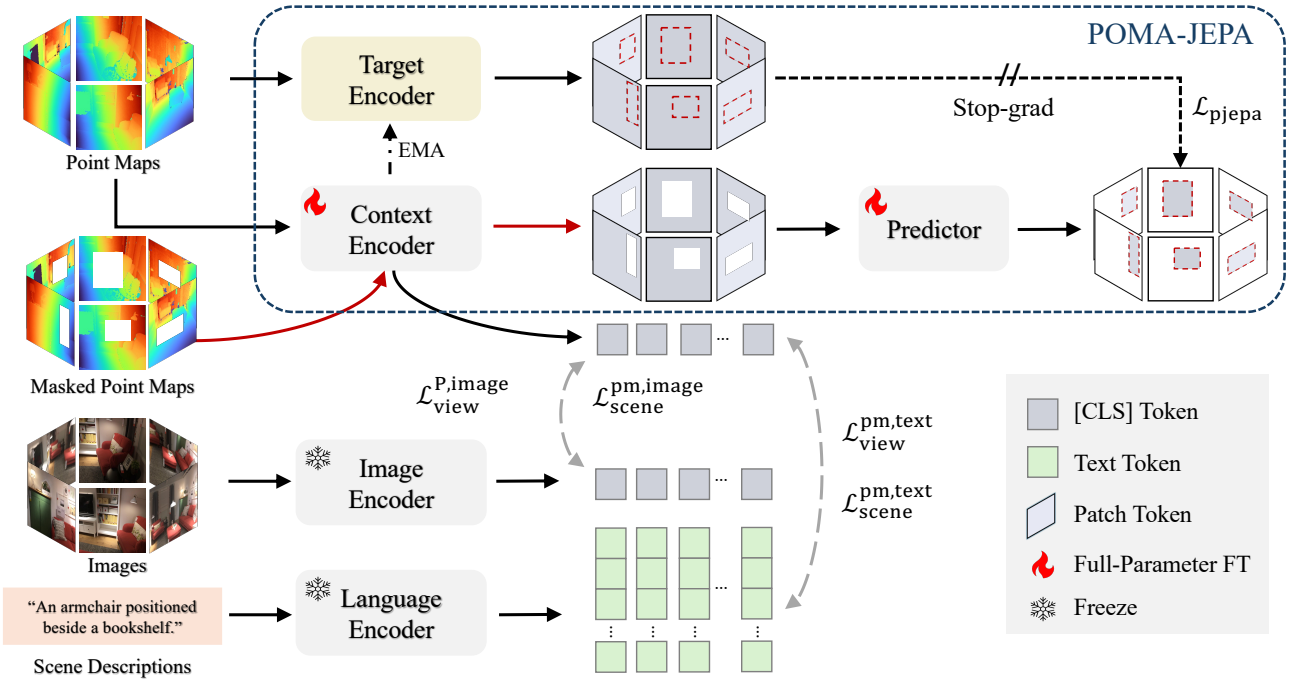

Figure 2. **Overview of the POMA-3D pretraining.** POMA-3D is pretrained with two objectives: (1) aligning [CLS] embeddings from the point map context encoder with image and text embeddings from the frozen FG-CLIP using $\mathcal{L}_{\text{view}}$ and $\mathcal{L}_{\text{scene}}$, and (2) reconstructing masked point map embeddings from the target encoder using unmasked embeddings from the context encoder via a predictor optimized by $\mathcal{L}_{\text{pjepa}}$. The target encoder is updated via EMA of the context encoder, and its final weights are used for downstream 3D understanding.

to enforce geometric consistency across multi-view point map embeddings. Frozen image and language encoders are aligned with a trainable point map context encoder. The context encoder, together with a predictor and an EMA-updated target encoder, optimizes POMA-JEPA. The features from the pretrained target encoder will finally be used for downstream analysis.

4.1. View-to-Scene Vision-Language Alignment

A scene consists of point maps $P = \{P_i\}_{i=1}^{N_v}$, images $I = \{I_i\}_{i=1}^{N_v}$, view-level captions $V = \{V_i\}_{i=1}^{N_v}$, and optionally a scene-level caption S, where N_v denotes the number of views. FG-CLIP [50] is chosen as the backbone for view-to-scene vision–language alignment due to its extended text token capacity, enabling effective modeling of long scene descriptions. Specifically, the alignment incorporates pretrained FG-CLIP image and language encoders E_I and E_L. A context point map encoder E_C, initialized from E_I and finetuned, is used to bridge 3D and 2D modalities.

For i_{th} view, the encoders produce modality-specific embeddings: $z_P^i = E_C(P_i)$, $z_I^i = E_I(I_i)$, and $z_V^i = E_L(V_i)$, where z_P^i, z_I^i, and z_V^i denote the [CLS] token embeddings of the point map, image, and per-view caption, respectively. The view-level alignment encourages each point map embedding to align with its paired image and caption embeddings while contrasting against different views in the batch, selected by the maximum coverage sampling. For any two modalities M_1 and M_2, the loss is:

$$\mathcal{L}_{\text{view}}^{M_1,M_2} = -\frac{1}{2}\sum_{(i,j)}\left(\log\frac{\exp\left(z_{M_1}^i \cdot z_{M2}^j/\tau\right)}{\sum_k \exp\left(z_{M_1}^i \cdot z_{M_2}^k/\tau\right)} + \log\frac{\exp\left(z_{M_1}^i \cdot z_{M_2}^j/\tau\right)}{\sum_k \exp\left(z_{M_1}^k \cdot z_{M_2}^j/\tau\right)}\right), \quad (2)$$

where (i,j) denotes a positive pair, while (i,k) and (k,j) represent negative pairs within the batch, and τ is the temperature parameter. Specifically, $\mathcal{L}_{\text{view}}^{P,I}$ aligns point map and image modalities ($M_1{=}P$, $M_2{=}I$), whereas $\mathcal{L}_{\text{view}}^{P,V}$ aligns point map and text modalities ($M_1{=}P$, $M_2{=}V$). The total view loss $\mathcal{L}_{\text{view}} = \mathcal{L}_{\text{view}}^{P,I} + \mathcal{L}_{\text{view}}^{P,V}$.

For scene-level alignment, point map and image embeddings $\{z_P^i\}_{i=1}^{N_v}$ and $\{z_I^i\}_{i=1}^{N_v}$ within each scene are mean-pooled into scene embeddings $\bar{z}_P$ and $\bar{z}_I$. The scene caption S is encoded as $\bar{z}_S = E_L(S)$. Each scene's point map embedding is aligned with its paired image and caption embeddings while contrasting against other scenes in the batch:

$$\mathcal{L}_{\text{scene}}^{M_1,M_2} = -\frac{1}{2}\sum_{(i,j)}\left(\log\frac{\exp\left(\bar{z}_{M_1}^i \cdot \bar{z}_{M_2}^j/\tau\right)}{\sum_k \exp\left(\bar{z}_{M_1}^i \cdot \bar{z}_{M_2}^k/\tau\right)} + \log\frac{\exp\left(\bar{z}_{M_1}^i \cdot \bar{z}_{M_2}^j/\tau\right)}{\sum_k \exp\left(\bar{z}_{M_1}^k \cdot \bar{z}_{M_2}^j/\tau\right)}\right), \quad (3)$$

where $\mathcal{L}_{\text{scene}}^{P,I}$ and $\mathcal{L}_{\text{scene}}^{P,S}$ denote scene-level point map–image and point map–caption alignments. $\mathcal{L}_{\text{scene}} = \mathcal{L}_{\text{scene}}^{P,I} + \mathcal{L}_{\text{scene}}^{P,S}$.

4.2. POMA-JEPA

As shown in Fig. 2, the POMA-JEPA pretraining module consists of a context encoder E_C, a target encoder E_T, and a predictor f_θ. Given multi-view point maps $\{P_i\}_{i=1}^{N_v}$, a random masking function $\mathcal{M}(\cdot)$ is applied to each view to mask a subset of patches. The union of all masked patches across views is denoted as Ω_M, and its visible complement is Ω_V (see appendix for examples). The context encoder encodes the visible regions from all views to obtain latent features $Z_C = \{E_C(P_i^{\Omega_V})\}_{i=1}^{N_v}$. The target encoder processes the complete point maps to produce full patch embeddings $Z_T = \{E_T(P_i)\}_{i=1}^{N_v}$. The predictor takes the concatenated context embeddings from all views to reconstruct the target embeddings of the masked regions, $\hat{Z}_T = f_\theta(Z_C)$. During POMA-JEPA training, the context encoder E_C continues fine-tuning, while the target encoder E_T is updated as the EMA of the context encoder E_C after each iteration.

Since the merged point maps in the world coordinate frame form a dense point cloud, it naturally inherits the order-agnostic nature of point sets. Consequently, the predicted patch embeddings $\hat{Z}_T$ do not necessarily follow the same spatial order as the target embeddings Z_T. The standard JEPA utilizes MSE loss that enforces a one-to-one mapping in a fixed 2D grid, which we find leads to mode collapse in the 3D setting. Here, we define the POMA-JEPA loss $\mathcal{L}_{\text{pjepa}}$ using the Chamfer Distance [14], a widely used metric in masked point cloud modeling [37] for its robustness to minor order misalignments, defined as:

$$\mathcal{L}_{\text{pjepa}} = \sum_i \min_j \|\hat{Z}_T^i - Z_T^j\|_2^2 + \sum_j \min_i \|Z_T^j - \hat{Z}_T^i\|_2^2, \quad (4)$$

where $i, j \in \Omega_M$ denote indices of masked patches.

4.3. Two-Stage Pretraining

POMA-3D is pretrained in two stages. The first **warm-up stage** performs vision–language alignment on all image-derived single-view point maps, with the total loss defined as $\mathcal{L}_{\text{total}} = \mathcal{L}_{\text{view}}$. The **main stage** jointly optimizes alignment and POMA-JEPA pretraining on multi-view point maps from room-level scenes. Both the context and target point map encoders are initialized from the context encoder weights obtained after the warm-up stage. The total loss for this stage is defined as:

$$\mathcal{L}_{\text{total}} = \mathcal{L}_{\text{view}} + \mathcal{L}_{\text{scene}} + \mathcal{L}_{\text{pjepa}}. \quad (5)$$

5. Experiments

5.1. Experimental Settings

Implementation Details. POMA-3D is pretrained for 20 epochs during the warm-up stage and 100 epochs in the main stage, with batch sizes of 1024 and 64, respectively. We adopt the AdamW [32] optimizer (β_1 = 0.9, β_2 = 0.98) with a learning rate of 1×10^{-4}, a warm-up of 500 steps, and cosine decay scheduling. The vision encoders are ViT-B/16 from FG-CLIP-Base [50]. For the POMA-JEPA, the predictor depth is set to 2, and each point map view is assigned a single mask with a random scale in the range $(0.15, 0.2)$ and an aspect ratio in the range $(0.75, 1.5)$. All data construction, pretraining, and downstream fine-tuning are conducted on A100 (80 GB) GPUs. More details are in the Appendix.

3D QA Setting. We evaluate our model on three benchmarks: the ScanQA [4] validation set, the SQA3D [33] test set, and the ScanNet split of Hypo3D [36], which assess commonsense spatial, situated, and hypothetical reasoning, respectively. The Hypo3D dataset is divided into training, validation, and test sets with an 8:1:1 ratio based on scene IDs. Based on the POMA-3D encoder, we develop two baselines: a specialist model, POMA-3D$_{\text{spec}}$, and a generalist model, POMA-3D$_{\text{llm}}$. POMA-3D$_{\text{spec}}$ follows 3D-VisTA [59] and SceneVerse [24], consisting of a BERT language encoder and a QA head, and is fine-tuned with QA loss. POMA-3D$_{\text{llm}}$ aligns the POMA-3D encoder with the LLaVA-OV LLM via one epoch of LoRA fine-tuning, following the same protocol as SplatTalk [44]. We compare POMA-3D$_{\text{spec}}$ and POMA-3D$_{\text{llm}}$ against three 3D LLMs, three 2D LLMs, and five specialist models. For fairness, all 2D LLMs, following POMA-3D, take 32-view images as input. 3D-VisTA [59], SceneVerse [24], and SplatTalk [44] are 3D VLL models fine-tuned on QA tasks and are most related to us. Since 3D-VisTA and SceneVerse additionally require object masks, evaluations on ScanQA and SQA3D employ masks generated by Mask3D [42], while Hypo3D uses ground-truth masks. For LLM-based models, we report exact match (EM@1) scores, and for specialist models, we report both EM@1 and EM@10 metrics.

Embodied Navigation Setting. The embodied navigation task is evaluated on the MSNN [30] dataset, which tests a model's ability to infer the correct navigational direction given the 3D scene, agent's situation, and task instruction (see Fig. 1). MSNN is divided into training, validation, and test sets with an 8:1:1 split. Models used for 3D QA are also applied to this task. Each sample provides answers at four- and eight-directional granularities (4-dir. and 8-dir.).

Scene Retrieval Setting. Ground-truth bounding boxes in existing 3D visual grounding (VG) datasets are defined on post-processed point clouds that are misaligned with point maps directly projected from depth maps, making direct evaluation of POMA-3D non-trivial. Instead, we repurpose existing 3D VG datasets, including ScanRefer [8], Nr3D, and Sr3D [1], for scene retrieval. In this task, the model retrieves the 3D scene given a scene description composed of referring texts from the dataset. Retrieval is performed by computing the similarity between the description embeddings and the mean-pooled point map embeddings, se-

Table 2. 3D QA results on ScanQA [4], SQA3D [33], and Hypo3D [36], and embodied navigation results on MSNN [30]. 4 dir./8 dir.:four/eight-directional navigation; C-PC: colored point cloud; RGB: image; RGB-D: image + depth; GS: Gaussian Splat; PM: point map. '†' indicates models with $H \times W \times 3$ grid inputs and LoRA-tuned for one epoch from the 2D LLM. '–' indicates the metric is inapplicable or the result is unavailable. **Best** and second-best 2D LLM-based and specialist model results are highlighted.

Method	Modality	ScanQA		SQA3D		Hypo3D		MSNN	
		EM@1	EM@10	EM@1	EM@10	EM@1	EM@10	4 dir.	8 dir.
3D LLM Models									
LEO [20]	C-PC	24.5	–	50.0	–	16.2	–	–	–
LLaVA-3D [57]	RGB-D	27.0	–	55.6	–	33.1	–	22.9	12.3
Video-3D LLM [54]	RGB-D	30.1	–	58.6	–	–	–	–	–
2D LLM-based Models (Pretrained/LoRA-tuned)									
Qwen2.5-VL-7B [5]	RGB	**23.7**	–	47.8	–	30.9	–	21.8	2.87
LLaVA-OV-7B [27]	RGB	20.8	–	47.7	–	33.2	–	24.0	5.83
SplatTalk† [44]	RGB(GS)	22.4	–	47.6	–	–	–	–	–
POMA-3D$^{\dagger}_{llm}$	PM	21.3	–	**51.6**	–	**35.9**	–	**36.9**	**21.4**
Specialist Models									
ScanQA [4]	C-PC	21.1	–	47.2	–	–	–	–	–
SQA3D [33]	C-PC	–	–	46.6	–	–	–	–	–
3D-ViSTA [59]	C-PC	22.4	52.1	48.5	85.6	31.0	81.2	39.9	20.1
SceneVerse [24]	C-PC	**22.7**	51.5	49.9	85.0	31.6	80.3	36.0	19.5
FG-CLIP [50]	PM	20.9	49.9	49.5	89.7	31.1	82.1	39.3	20.4
POMA-3D$_{spec}$	**PM**	22.3	**52.3**	**51.1**	**91.2**	**33.4**	**84.8**	**40.4**	**21.2**

Table 3. Scene retrieval results on ScanRefer [8], Nr3D, and Sr3D [1]. The metric R@M-N denotes recall@N for retrieving the correct 3D scene from M referring texts. All methods are evaluated in the zero-shot setting. **Best** and second-best results are highlighted.

Method	Modality	ScanRefer				Nr3D				Sr3D			
		R@1-1	R@1-5	R@5-1	R@5-5	R@1-1	R@1-5	R@5-1	R@5-5	R@1-1	R@1-5	R@5-1	R@5-5
3D-ViSTA [59]	C-PC	0.48	2.27	0.24	2.03	0.45	0.60	0.15	0.60	0.33	1.15	0.33	1.48
SceneVerse [24]	C-PC	0.24	2.27	0.83	2.03	0.26	1.82	0.26	1.56	0.28	1.99	0.28	1.70
FG-CLIP [50]	RGB	5.10	16.4	14.9	42.2	1.37	6.71	5.18	17.2	1.35	6.42	1.86	10.1
FG-CLIP [50]	PM	0.50	2.00	0.25	2.81	0.46	1.98	0.46	2.13	0.34	1.18	0.17	0.84
POMA-3D	PM	**9.31**	**27.9**	**29.4**	**59.4**	**8.10**	**15.7**	**15.0**	**42.2**	**3.89**	**14.0**	**6.59**	**20.7**

lecting the scene with the highest similarity. We compare POMA-3D against 3D-VisTA [59], SceneVerse [24], and FG-CLIP [50]. Performance is reported using R@M–N, where M is the number of referring texts composing the scene description and N is the Top-N recall.

Coarse Localization Setting. The view-level alignment enables POMA-3D to retrieve point map views matching the agent's location (i.e., coarse localization). Specifically, the similarity between each point map view embedding within a scene and the situational text embedding (e.g., "I am sitting on the bed") is computed. The Top-K most similar point maps are retrieved. When all point maps in the scene are concatenated, the retrieved ones collectively highlight the agent's active region in the world frame. We qualitatively evaluate coarse localization with $K = 3$.

5.2. Downstream Task Results

3D QA. As shown in Tab. 2, our specialist model POMA-3D$_{spec}$ outperforms all evaluated specialist models on the SQA3D and Hypo3D datasets. However, it does not outperform all methods on ScanQA, likely because ScanQA contains a number of color-dependent questions. Comparison models leverage color inputs (e.g., colored point clouds or images), while our input is uncolored point maps that lack such cues. Additionally, POMA-3D$_{spec}$ exhibits consistent gains in EM@10, surpassing all models across datasets. In particular, it outperforms the state-of-the-art point cloud–based VLL model SceneVerse by 6.2% on SQA3D and 4.5% on Hypo3D. Even when compared to large 3D LLMs such as LEO and LLaVA-3D, POMA-3D$_{spec}$ still achieves noticeable improvements on Hypo3D. Relative to its FG-CLIP baseline, POMA-3D$_{spec}$ further improves EM@1 and EM@10 by around 2% on all benchmarks, confirming the effectiveness of the proposed pretraining strategy. Furthermore, POMA-3D$_{llm}$ outperforms existing 2D LLMs on both SQA3D and Hypo3D. Compared to SplatTalk, POMA-3D$_{llm}$ achieves a 4% improvement on SQA3D, illustrating the superiority of point map representation over 3DGS for situational reasoning.

Embodied Navigation. Tab. 2 demonstrates that among all

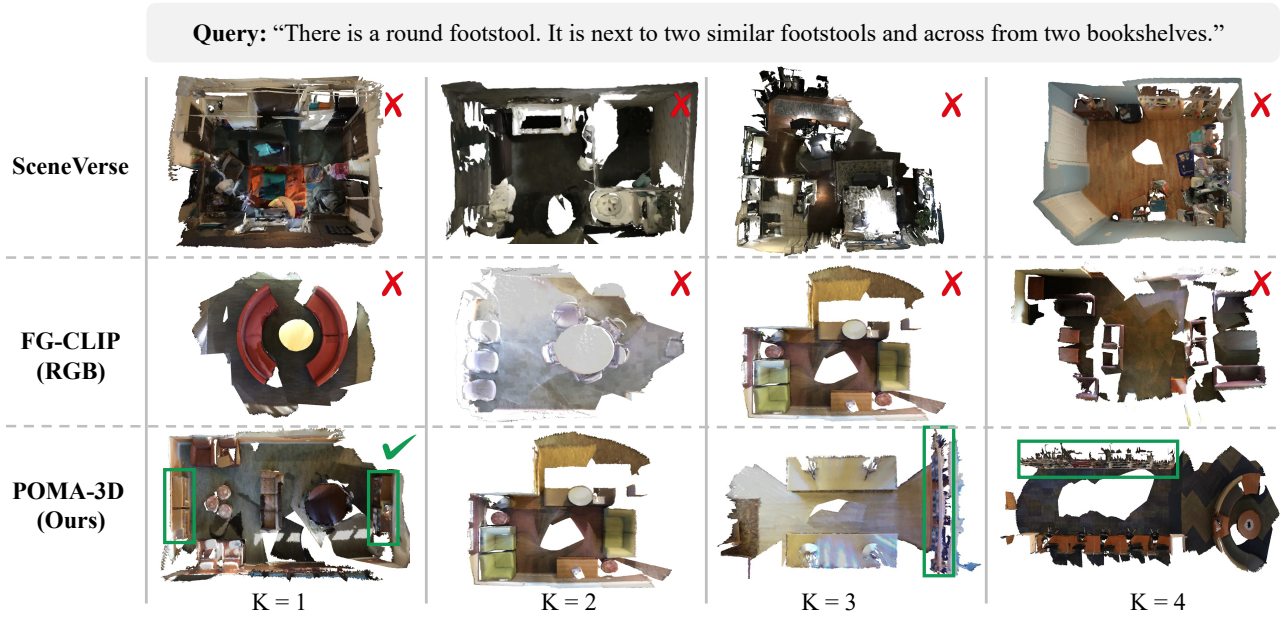

Figure 3. **Qualitative scene retrieval results.** Top-4 candidates from each method are shown. For the given query, only POMA-3D retrieves the unique ground-truth scene, while others fail to return bookshelf-containing scenes. Green boxes mark bookshelves.

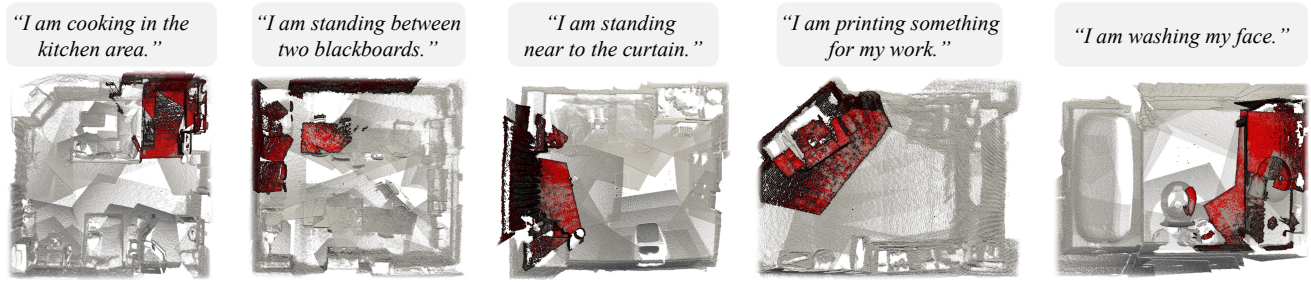

Figure 4. **Qualitative coarse localization results.** Top: text to describe the current agent's situation. Bottom: merged multi-view point maps, where red regions indicate the point map views retrieved by POMA-3D based on the text.

models, POMA-3D$_{\text{spec}}$ achieves the highest performance on four-directional navigation, while POMA-3D$_{\text{llm}}$ performs best on eight-directional navigation. This indicates that POMA-3D's advantage becomes more pronounced when requiring complex spatial reasoning beyond simple relationship and attribute recognition in traditional 3D QA.

Scene Retrieval. Tab. 3 presents the quantitative results for scene retrieval. POMA-3D consistently outperforms its FG-CLIP baseline and all 3D VLL methods across datasets and metrics. Notably, prior approaches underperform the RGB-based FG-CLIP model, and in some metrics, even below its point map variant, despite FG-CLIP being pretrained solely on image data. This is likely because these methods align a newly trained point encoder with a BERT text encoder, failing to leverage the strong priors in pre-aligned CLIP. In contrast, POMA-3D builds upon the pretrained FG-CLIP, effectively extending its image–text alignment to point map–text alignment. Fig. 3 further qualitatively demonstrates our method's superiority. For a query requiring three footstools and bookshelves, only POMA-3D retrieves the single correct scene and returns bookshelf-containing results in three of the top four matches (green boxes), while all other methods fail to meet the query conditions.

Coarse Localization. Qualitative results in Fig. 4 show that POMA-3D accurately retrieves point map views describing the agent's position from situational text containing multiple objects. For example, given "I am standing between two blackboards," it correctly identifies the intersection area. It also performs well when no object references in queries, such as in "I am washing my face," where it locates the basin area, demonstrating strong situational reasoning.

5.3. Ablation Studies

Effect of Warmup with 2D Data. Tab. 4 presents the ablations of POMA-3D components across 3D QA datasets. The first row, without any pretraining, corresponds to the

Table 4. Ablation study of POMA-3D on 3D QA datasets.

Warmup	Main			EM@1		
$\mathcal{L}_{view}$	$\mathcal{L}_{view}$	$\mathcal{L}_{scene}$	$\mathcal{L}_{pjepa}$	ScanQA	SQA3D	Hypo3D
✗	✗	✗	✗	20.9	49.5	31.1
✓	✗	✗	✗	20.6	50.1	32.4
✗	✓	✓	✗	21.4	50.4	32.6
✓	✓	✓	✗	22.1	50.7	32.9
✓	✓	✓	✓	**22.3**	**51.1**	**33.4**

Table 5. Ablation study of FG-CLIP and POMA-3D as visual encoders for LLaVA-OV. Both models were pretrained on SQA3D [33] and evaluated zero-shot on Hypo3D [36].

Visual Encoder	Scale	Direction	Semantic	Overall
FG-CLIP [50]	44.1	15.2	33.3	30.3
POMA-3D	**45.3**	**16.7**	**33.6**	**30.9**

FG-CLIP finetuned on the downstream tasks. Warmup pretraining on point maps derived from images improves EM@1 by 0.6% on SQA3D and 1.3% on Hypo3D. When combined with the main stage, the warmup further boosts ScanQA by 0.7%. Hence, pretraining on 2D-derived point maps makes POMA-3D learn more robust 3D features.

Effect of the Room-Level Scenes. Consistent with prior 3D VLL methods, incorporating room scenes benefits POMA-3D pretraining. As shown in the third row of Tab.4, room-level alignment with $\mathcal{L}_{view}$ and $\mathcal{L}_{scene}$ boots EM@1 across all benchmarks, surpassing all specialist models and several LLM-based methods on Hypo3D (See Tab.2).

Effect of POMA-JEPA. Tab. 4 shows that incorporating the POMA-JEPA training objective consistently improves POMA-3D performance across all benchmarks, with the largest gains observed on SQA3D and Hypo3D. These results suggest that enforcing geometric consistency across multi-view features further strengthens POMA-3D's capability in situated and hypothetical reasoning.

Zero-Shot Generalization of POMA-3D. All results above evaluate POMA-3D under fine-tuning on downstream benchmarks. Tab. 5 further presents cross-dataset results, comparing FG-CLIP and POMA-3D as visual encoders within LLaVA-OV. Both models are fine-tuned on SQA3D and evaluated zero-shot on Hypo3D. The POMA-3D–based LLaVA-OV achieves higher overall EM@1, with gains of 1.2% and 1.5% on scale and direction questions, respectively (i.e., spatial questions). These results demonstrate that POMA-3D features transfer effectively across tasks.

Effect of the Number of Point Map Views. We evaluate POMA-3D under different numbers of views used during finetuning on SQA3D task. As shown in Fig. 5, POMA-3D consistently outperforms the FG-CLIP across all view counts on EM@1 and EM@10. Unlike FG-CLIP, which plateaus or declines with more views, POMA-3D improves steadily, showing that each point map view in POMA-3D provides complementary features.

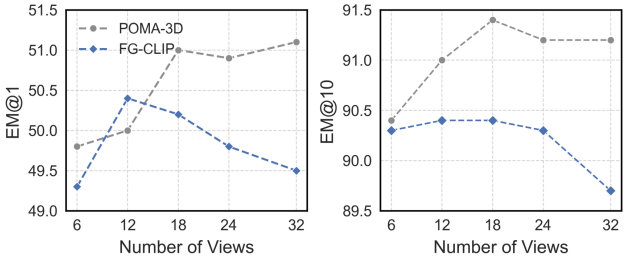

Figure 5. Comparison of POMA-3D and its baseline FG-CLIP with varying numbers of views on SQA3D [33].

Table 6. 3D QA performance of pretrained and aligned FG-CLIP models using depth maps and point maps as input.

Modality	$\mathcal{L}_{view}$ $\mathcal{L}_{scene}$	ScanQA	SQA3D	Hypo3D
Depth Map	✗	20.1	49.1	31.0
	✓	21.0	50.1	31.5
Point Map	✗	20.9	49.5	31.1
	✓	**21.4**	**50.4**	**32.6**

Comparing Point Map with Other 3D Modalities. This experiment hypothesizes that the point map is a more effective 3D modality for representation learning. Tab. 6 compares pretrained FG-CLIP models using point maps and depth maps as inputs for 3D QA. Point maps yield consistently better results, suggesting that 2D priors transfer more effectively to point maps. This advantage persists even when both modalities are aligned with $\mathcal{L}_{view}$ and $\mathcal{L}_{scene}$. Moreover, point map features receive additional gains from POMA-JEPA, while depth maps do not. Tab. 2 further shows that POMA-3D surpasses point cloud– and GS-based methods. Altogether, these findings highlight point maps as a more promising 3D modality for feature learning.

6. Conclusion

In this work, we introduce POMA-3D, the first point map-based self-supervised 3D model. Pretrained on the Scene-Point dataset using view-to-scene vision–language alignment and POMA-JEPA objectives, POMA-3D learns robust point map representations that generalize to diverse 3D tasks. The learned features strengthen both lightweight specialist and large generalist 3D models. Importantly, POMA-3D effectively inherits priors from 2D foundation models and benefits from large-scale image datasets. We believe this work paves the way to scalable 3D understanding.

Limitation. Since point maps contain only coordinates, future work should explore fusing them with color features to build a unified scene representation.

7. Acknowledgments

Supported by the Imperial President's Scholarship.

References

[1] Panos Achlioptas, Ahmed Abdelreheem, Fei Xia, Mohamed Elhoseiny, and Leonidas Guibas. Referit3d: Neural listeners for fine-grained 3d object identification in real-world scenes. In *European conference on computer vision*, pages 422–440. Springer, 2020. 1, 5, 6

[2] Mahmoud Assran, Quentin Duval, Ishan Misra, Piotr Bojanowski, Pascal Vincent, Michael Rabbat, Yann LeCun, and Nicolas Ballas. Self-supervised learning from images with a joint-embedding predictive architecture. In *Proceedings of the IEEE/CVF Conference on Computer Vision and Pattern Recognition*, pages 15619–15629, 2023. 2

[3] Mido Assran, Adrien Bardes, David Fan, Quentin Garrido, Russell Howes, Matthew Muckley, Ammar Rizvi, Claire Roberts, Koustuv Sinha, Artem Zholus, et al. V-jepa 2: Self-supervised video models enable understanding, prediction and planning. *arXiv preprint arXiv:2506.09985*, 2025. 2

[4] Daichi Azuma, Taiki Miyanishi, Shuhei Kurita, and Motoaki Kawanabe. Scanqa: 3d question answering for spatial scene understanding. In *proceedings of the IEEE/CVF conference on computer vision and pattern recognition*, pages 19129–19139, 2022. 1, 5, 6

[5] Shuai Bai, Keqin Chen, Xuejing Liu, Jialin Wang, Wenbin Ge, Sibo Song, Kai Dang, Peng Wang, Shijie Wang, Jun Tang, et al. Qwen2. 5-vl technical report. *arXiv preprint arXiv:2502.13923*, 2025. 6

[6] Adrien Bardes, Quentin Garrido, Jean Ponce, Xinlei Chen, Michael Rabbat, Yann LeCun, Mido Assran, and Nicolas Ballas. V-jepa: Latent video prediction for visual representation learning. 2023. 2

[7] Gilad Baruch, Zhuoyuan Chen, Afshin Dehghan, Tal Dimry, Yuri Feigin, Peter Fu, Thomas Gebauer, Brandon Joffe, Daniel Kurz, Arik Schwartz, et al. Arkitscenes: A diverse real-world dataset for 3d indoor scene understanding using mobile rgb-d data. *arXiv preprint arXiv:2111.08897*, 2021. 3

[8] Dave Zhenyu Chen, Angel X Chang, and Matthias Nießner. Scanrefer: 3d object localization in rgb-d scans using natural language. In *European conference on computer vision*, pages 202–221. Springer, 2020. 1, 2, 5, 6

[9] Sijin Chen, Xin Chen, Chi Zhang, Mingsheng Li, Gang Yu, Hao Fei, Hongyuan Zhu, Jiayuan Fan, and Tao Chen. Ll3da: Visual interactive instruction tuning for omni-3d understanding reasoning and planning. In *Proceedings of the IEEE/CVF conference on computer vision and pattern recognition*, pages 26428–26438, 2024. 1

[10] An-Chieh Cheng, Yang Fu, Yukang Chen, Zhijian Liu, Xiaolong Li, Subhashree Radhakrishnan, Song Han, Yao Lu, Jan Kautz, Pavlo Molchanov, et al. 3d aware region prompted vision language model. *arXiv preprint arXiv:2509.13317*, 2025. 2

[11] Angela Dai, Angel X Chang, Manolis Savva, Maciej Halber, Thomas Funkhouser, and Matthias Nießner. Scannet: Richly-annotated 3d reconstructions of indoor scenes. In *Proceedings of the IEEE conference on computer vision and pattern recognition*, pages 5828–5839, 2017. 3

[12] Matt Deitke, Eli VanderBilt, Alvaro Herrasti, Luca Weihs, Kiana Ehsani, Jordi Salvador, Winson Han, Eric Kolve, Aniruddha Kembhavi, and Roozbeh Mottaghi. Procthor: Large-scale embodied ai using procedural generation. *Advances in Neural Information Processing Systems*, 35:5982–5994, 2022. 3

[13] Jiafei Duan, Samson Yu, Hui Li Tan, Hongyuan Zhu, and Cheston Tan. A survey of embodied ai: From simulators to research tasks. *IEEE Transactions on Emerging Topics in Computational Intelligence*, 6(2):230–244, 2022. 1

[14] Haoqiang Fan, Hao Su, and Leonidas J Guibas. A point set generation network for 3d object reconstruction from a single image. In *Proceedings of the IEEE conference on computer vision and pattern recognition*, pages 605–613, 2017. 5

[15] Zhiwen Fan, Jian Zhang, Renjie Li, Junge Zhang, Runjin Chen, Hezhen Hu, Kevin Wang, Huaizhi Qu, Dilin Wang, Zhicheng Yan, et al. Vlm-3r: Vision-language models augmented with instruction-aligned 3d reconstruction. *arXiv preprint arXiv:2505.20279*, 2025. 1

[16] Rao Fu, Jingyu Liu, Xilun Chen, Yixin Nie, and Wenhan Xiong. Scene-llm: Extending language model for 3d visual understanding and reasoning. *arXiv preprint arXiv:2403.11401*, 2024. 1

[17] Zoey Guo, Yiwen Tang, Ray Zhang, Dong Wang, Zhigang Wang, Bin Zhao, and Xuelong Li. Viewrefer: Grasp the multi-view knowledge for 3d visual grounding. In *Proceedings of the IEEE/CVF International Conference on Computer Vision*, pages 15372–15383, 2023. 2

[18] Yining Hong, Haoyu Zhen, Peihao Chen, Shuhong Zheng, Yilun Du, Zhenfang Chen, and Chuang Gan. 3d-llm: Injecting the 3d world into large language models. *Advances in Neural Information Processing Systems*, 36:20482–20494, 2023. 2

[19] Ji Hou, Angela Dai, and Matthias Nießner. 3d-sis: 3d semantic instance segmentation of rgb-d scans. In *Proceedings of the IEEE/CVF conference on computer vision and pattern recognition*, pages 4421–4430, 2019. 1, 2

[20] Jiangyong Huang, Silong Yong, Xiaojian Ma, Xiongkun Linghu, Puhao Li, Yan Wang, Qing Li, Song-Chun Zhu, Baoxiong Jia, and Siyuan Huang. An embodied generalist agent in 3d world. *arXiv preprint arXiv:2311.12871*, 2023. 2, 6

[21] Ranran Huang and Krystian Mikolajczyk. No pose at all: Self-supervised pose-free 3d gaussian splatting from sparse views. In *Proceedings of the IEEE/CVF International Conference on Computer Vision*, pages 27947–27957, 2025. 2

[22] Shijia Huang, Yilun Chen, Jiaya Jia, and Liwei Wang. Multi-view transformer for 3d visual grounding. In *Proceedings of the IEEE/CVF Conference on Computer Vision and Pattern Recognition*, pages 15524–15533, 2022. 2

[23] Tianyu Huang, Bowen Dong, Yunhan Yang, Xiaoshui Huang, Rynson WH Lau, Wanli Ouyang, and Wangmeng Zuo. Clip2point: Transfer clip to point cloud classification with image-depth pre-training. In *Proceedings of the IEEE/CVF International Conference on Computer Vision*, pages 22157–22167, 2023. 2

[24] Baoxiong Jia, Yixin Chen, Huangyue Yu, Yan Wang, Xuesong Niu, Tengyu Liu, Qing Li, and Siyuan Huang.

Sceneverse: Scaling 3d vision-language learning for grounded scene understanding. In *European Conference on Computer Vision*, pages 289–310. Springer, 2024. 2, 3, 5, 6

[25] Li Jiang, Hengshuang Zhao, Shaoshuai Shi, Shu Liu, Chi-Wing Fu, and Jiaya Jia. Pointgroup: Dual-set point grouping for 3d instance segmentation. In *Proceedings of the IEEE/CVF conference on computer vision and Pattern recognition*, pages 4867–4876, 2020. 1, 2

[26] Vincent Leroy, Yohann Cabon, and Jérôme Revaud. Grounding image matching in 3d with mast3r. In *European Conference on Computer Vision*, pages 71–91. Springer, 2024. 2

[27] Bo Li, Yuanhan Zhang, Dong Guo, Renrui Zhang, Feng Li, Hao Zhang, Kaichen Zhang, Peiyuan Zhang, Yanwei Li, Ziwei Liu, et al. Llava-onevision: Easy visual task transfer. *arXiv preprint arXiv:2408.03326*, 2024. 6

[28] Yue Li, Qi Ma, Runyi Yang, Huapeng Li, Mengjiao Ma, Bin Ren, Nikola Popovic, Nicu Sebe, Ender Konukoglu, Theo Gevers, et al. Scenesplat: Gaussian splatting-based scene understanding with vision-language pretraining. *arXiv preprint arXiv:2503.18052*, 2025. 2, 3

[29] Zechuan Li, Hongshan Yu, Yihao Ding, Yan Li, Yong He, and Naveed Akhtar. Embodied intelligence for 3d understanding: A survey on 3d scene question answering. *arXiv preprint arXiv:2502.00342*, 2025. 1

[30] Xiongkun Linghu, Jiangyong Huang, Xuesong Niu, Xiaojian Shawn Ma, Baoxiong Jia, and Siyuan Huang. Multi-modal situated reasoning in 3d scenes. *Advances in Neural Information Processing Systems*, 37:140903–140936, 2024. 5, 6

[31] Minghua Liu, Ruoxi Shi, Kaiming Kuang, Yinhao Zhu, Xuanlin Li, Shizhong Han, Hong Cai, Fatih Porikli, and Hao Su. Openshape: Scaling up 3d shape representation towards open-world understanding. *Advances in neural information processing systems*, 36:44860–44879, 2023. 2

[32] Ilya Loshchilov and Frank Hutter. Decoupled weight decay regularization. *arXiv preprint arXiv:1711.05101*, 2017. 5

[33] Xiaojian Ma, Silong Yong, Zilong Zheng, Qing Li, Yitao Liang, Song-Chun Zhu, and Siyuan Huang. Sqa3d: Situated question answering in 3d scenes. *arXiv preprint arXiv:2210.07474*, 2022. 1, 5, 6, 8

[34] Yongsen Mao, Yiming Zhang, Hanxiao Jiang, Angel Chang, and Manolis Savva. Multiscan: Scalable rgbd scanning for 3d environments with articulated objects. *Advances in neural information processing systems*, 35:9058–9071, 2022. 3

[35] Ye Mao, Junpeng Jing, and Krystian Mikolajczyk. Opendlign: Open-world point cloud understanding with depth-aligned images. *Advances in Neural Information Processing Systems*, 37:101144–101167, 2024. 2

[36] Ye Mao, Weixun Luo, Junpeng Jing, Anlan Qiu, and Krystian Mikolajczyk. Hypo3d: Exploring hypothetical reasoning in 3d. *arXiv preprint arXiv:2502.00954*, 2025. 5, 6, 8

[37] Yatian Pang, Eng Hock Francis Tay, Li Yuan, and Zhenghua Chen. Masked autoencoders for 3d point cloud self-supervised learning. *World Scientific Annual Review of Artificial Intelligence*, 1:2440001, 2023. 5

[38] Charles R Qi, Hao Su, Kaichun Mo, and Leonidas J Guibas. Pointnet: Deep learning on point sets for 3d classification and segmentation. In *Proceedings of the IEEE conference on computer vision and pattern recognition*, pages 652–660, 2017. 2

[39] Zekun Qi, Runpei Dong, Shaochen Zhang, Haoran Geng, Chunrui Han, Zheng Ge, Li Yi, and Kaisheng Ma. Shapellm: Universal 3d object understanding for embodied interaction. In *European Conference on Computer Vision*, pages 214–238. Springer, 2024. 2

[40] Alec Radford, Jong Wook Kim, Chris Hallacy, Aditya Ramesh, Gabriel Goh, Sandhini Agarwal, Girish Sastry, Amanda Askell, Pamela Mishkin, Jack Clark, et al. Learning transferable visual models from natural language supervision. In *International conference on machine learning*, pages 8748–8763. PmLR, 2021. 2

[41] Santhosh K Ramakrishnan, Aaron Gokaslan, Erik Wijmans, Oleksandr Maksymets, Alex Clegg, John Turner, Eric Undersander, Wojciech Galuba, Andrew Westbury, Angel X Chang, et al. Habitat-matterport 3d dataset (hm3d): 1000 large-scale 3d environments for embodied ai. *arXiv preprint arXiv:2109.08238*, 2021. 3

[42] Jonas Schult, Francis Engelmann, Alexander Hermans, Or Litany, Siyu Tang, and Bastian Leibe. Mask3d: Mask transformer for 3d semantic instance segmentation. *arXiv preprint arXiv:2210.03105*, 2022. 5

[43] Piyush Sharma, Nan Ding, Sebastian Goodman, and Radu Soricut. Conceptual captions: A cleaned, hypernymed, image alt-text dataset for automatic image captioning. In *Proceedings of the 56th Annual Meeting of the Association for Computational Linguistics (Volume 1: Long Papers)*, pages 2556–2565, 2018. 3

[44] Anh Thai, Songyou Peng, Kyle Genova, Leonidas Guibas, and Thomas Funkhouser. Splattalk: 3d vqa with gaussian splatting. *arXiv preprint arXiv:2503.06271*, 2025. 2, 5, 6

[45] Johanna Wald, Armen Avetisyan, Nassir Navab, Federico Tombari, and Matthias Nießner. Rio: 3d object instance relocalization in changing indoor environments. In *Proceedings of the IEEE/CVF International Conference on Computer Vision*, pages 7658–7667, 2019. 3

[46] Haochen Wang, Yucheng Zhao, Tiancai Wang, Haoqiang Fan, Xiangyu Zhang, and Zhaoxiang Zhang. Ross3d: Reconstructive visual instruction tuning with 3d-awareness. *arXiv preprint arXiv:2504.01901*, 2025. 1

[47] Jianyuan Wang, Minghao Chen, Nikita Karaev, Andrea Vedaldi, Christian Rupprecht, and David Novotny. Vggt: Visual geometry grounded transformer. In *Proceedings of the Computer Vision and Pattern Recognition Conference*, pages 5294–5306, 2025. 2, 3

[48] Shuzhe Wang, Vincent Leroy, Yohann Cabon, Boris Chidlovskii, and Jerome Revaud. Dust3r: Geometric 3d vision made easy. In *Proceedings of the IEEE/CVF Conference on Computer Vision and Pattern Recognition*, pages 20697–20709, 2024. 2

[49] Zehan Wang, Haifeng Huang, Yang Zhao, Ziang Zhang, and Zhou Zhao. Chat-3d: Data-efficiently tuning large language model for universal dialogue of 3d scenes. *arXiv preprint arXiv:2308.08769*, 2023. 2

[50] Chunyu Xie, Bin Wang, Fanjing Kong, Jincheng Li, Dawei Liang, Gengshen Zhang, Dawei Leng, and Yuhui Yin. Fg-

clip: Fine-grained visual and textual alignment. *arXiv preprint arXiv:2505.05071*, 2025. 3, 4, 5, 6, 8

[51] Le Xue, Mingfei Gao, Chen Xing, Roberto Martín-Martín, Jiajun Wu, Caiming Xiong, Ran Xu, Juan Carlos Niebles, and Silvio Savarese. Ulip: Learning a unified representation of language, images, and point clouds for 3d understanding. In *Proceedings of the IEEE/CVF conference on computer vision and pattern recognition*, pages 1179–1189, 2023. 2

[52] Le Xue, Ning Yu, Shu Zhang, Artemis Panagopoulou, Junnan Li, Roberto Martín-Martín, Jiajun Wu, Caiming Xiong, Ran Xu, Juan Carlos Niebles, et al. Ulip-2: Towards scalable multimodal pre-training for 3d understanding. In *Proceedings of the IEEE/CVF Conference on Computer Vision and Pattern Recognition*, pages 27091–27101, 2024. 2

[53] Hengshuang Zhao, Li Jiang, Jiaya Jia, Philip HS Torr, and Vladlen Koltun. Point transformer. In *Proceedings of the IEEE/CVF international conference on computer vision*, pages 16259–16268, 2021. 2

[54] Duo Zheng, Shijia Huang, and Liwei Wang. Video-3d llm: Learning position-aware video representation for 3d scene understanding. In *Proceedings of the Computer Vision and Pattern Recognition Conference*, pages 8995–9006, 2025. 1, 2, 3, 6

[55] Jia Zheng, Junfei Zhang, Jing Li, Rui Tang, Shenghua Gao, and Zihan Zhou. Structured3d: A large photo-realistic dataset for structured 3d modeling. In *European Conference on Computer Vision*, pages 519–535. Springer, 2020. 3

[56] Junsheng Zhou, Jinsheng Wang, Baorui Ma, Yu-Shen Liu, Tiejun Huang, and Xinlong Wang. Uni3d: Exploring unified 3d representation at scale. *arXiv preprint arXiv:2310.06773*, 2023. 2

[57] Chenming Zhu, Tai Wang, Wenwei Zhang, Jiangmiao Pang, and Xihui Liu. Llava-3d: A simple yet effective pathway to empowering lmms with 3d-awareness. *arXiv preprint arXiv:2409.18125*, 2024. 1, 2, 6

[58] Jinguo Zhu, Weiyun Wang, Zhe Chen, Zhaoyang Liu, Shenglong Ye, Lixin Gu, Hao Tian, Yuchen Duan, Weijie Su, Jie Shao, et al. Internvl3: Exploring advanced training and test-time recipes for open-source multimodal models. *arXiv preprint arXiv:2504.10479*, 2025. 3

[59] Ziyu Zhu, Xiaojian Ma, Yixin Chen, Zhidong Deng, Siyuan Huang, and Qing Li. 3d-vista: Pre-trained transformer for 3d vision and text alignment. In *Proceedings of the IEEE/CVF International Conference on Computer Vision*, pages 2911–2921, 2023. 2, 3, 5, 6